Measurement of low-lying states in ^{9}B

M.A. Tiede, K.W. Kemper, N.R. Fletcher, and D. Robson
Department of Physics, Florida State University, Tallahassee, Florida 32306

D.D. Caussyn
Indiana University Cyclotron Facility, Indiana University, Bloomington, Indiana 47405

S.J. Bennett
School of Physics and Space Research, University of Birmingham, Birmingham B15 2TT, United Kingdom

J.D. Brown
Joseph Henry Laboratories, Princeton University, Princeton, New Jersey 08544

W.N. Catford
Department of Physics, University of Surrey, Guildford GU2 5XH, United Kingdom

C.D. Jones and D.L. Watson
University of York, York YO1 5DD, United Kingdom

W.D.M. Rae
Department of Physics, University of Oxford, Nuclear Physics Laboratory, Keble Road, Oxford OX1 3RH, United Kingdom

(Received 15 December 1994)

A measurement of low-lying states in ^{9}B was conducted using the ^{6}Li(^{6}Li,t)^{9}B reaction at a beam energy of 56 MeV. The particles resulting from the decay of ^{9}B into ^{8}Be + p were detected with position sensitive detectors, and relative energy spectra were obtained from the data using the technique of resonant particle decay spectroscopy. This technique provided a very low background, and the ability to separate the ^{9}B states that decay by ^{8}Be + p from those that decay by ^{5}Li + α. Results show that a significant portion of the measured spectrum below $\approx$ 1.5 MeV cannot be explained by the known states which suggests that these counts arise from the mirror of the 1.68 MeV $\frac{1}{2}^+$ state of ^{9}Be. It was also shown that the recently observed $\frac{1}{2}^-$ state decays via the $p+^8$Be channel.

PACS number(s): 21.10.Pc, 23.50.+z, 27.20.+n, 25.70.Hi

I. INTRODUCTION

The study of mirror nuclear partners, i.e., nuclei which have the same number of nucleons except that the number of protons in one is equal to the number of neutrons in the other and vice versa ($N_1=Z_2, Z_1=N_2$), is important because it yields direct evidence about the charge independence of the nuclear force. The mirror pair that has posed the greatest mystery over the past 30 years is the mass 9 system. There has been considerable experimental and theoretical effort to determine the location of the low-lying states of ^{9}B, specifically the first excited $\frac{1}{2}^+$ state and the higher-lying $\frac{1}{2}^-$ state. These states are well known in the mirror nucleus ^{9}Be.

Widely varying measurements of the ^{9}B excitation energies have been reported for the first excited $\frac{1}{2}^+$ state ranging from E_{ex} = 1.16 ± 0.05 MeV with a width Γ = 1.30 ± 0.05 MeV using the ^{9}Be(^{3}He,t) reaction [1] to E_{ex} = 1.8 ± 0.2 MeV with a width Γ = 0.8 ± 0.3 MeV using the ^{10}B(^{3}He,α) reaction [2]. The situation is further confused by conflicting reports [3,4] concerning the observation of the $\frac{1}{2}^+$ state with the reaction ^{9}Be(^{6}Li,^{6}He). Thus the location and existence of the $\frac{1}{2}^+$ state are unclear. The higher-lying $\frac{1}{2}^-$ state has been observed in a recent ^{9}Be(p,n) work by Pugh [5]. However, the decay channels which depopulate this state are unknown, although the $p+^8$Be channel is a strong candidate since the ^{9}Be mirror state decays via $n+^8$Be.

Recent theoretical studies of the first excited state in ^{9}B also disagree on the excitation energy of the first excited $\frac{1}{2}^+$ state. Sherr and Bertsch [6] performed a calculation of Coulomb energies of unbound single-particle states in ^{9}B, and predicted the $\frac{1}{2}^+$ state to lie at E_{ex}=0.9 MeV with a large width of Γ = 1.4 MeV. This result corresponds to a large normal Thomas-Ehrman [7,8] shift. However, Barker [9] predicts an excitation energy $E_{ex} \approx$ 1.8 MeV in ^{9}B, i.e., higher than that of the mirror nucleus ^{9}Be. This ^{9}B excitation energy corresponds to an inverted Thomas-Ehrman shift.

The difficulty in locating these states experimentally occurs because ^{9}B is unbound, and its low-lying excited states are, for the most part, broad. The strongly excited $\frac{5}{2}^-$ state at 2.36 MeV will obscure the presence of the $\frac{1}{2}^+$ and $\frac{1}{2}^-$ states if their energies are close to it. By doing a triple coincidence experiment in which the energies and positions of the proton and two alpha particles resulting from the decay of the ^{9}B are measured, it is possible to separate the ^{9}B decay into p + ^{8}Be from ^{5}Li + α even though these two channels contain the same particles in their final states. Since the $\frac{5}{2}^-$ state decays $\geq$ 95% [10] via the ^{5}Li + α channel, it will be

removed from the ^{9}B spectrum obtained from the $p + {}^8$Be channel. This separation was accomplished in the present work by using position sensitive detectors and the technique of resonant particle decay spectroscopy (RPDS) to reconstruct the events and obtain the excitation energies of the states in ^{9}B for each reaction channel. The count rate for this triple coincidence experiment was small; therefore an array of four position sensitive detectors was utilized with the detector placement chosen to maximize the efficiency for the excitation region of interest.

The reaction ^{6}Li(^{6}Li,t)^{9}B was chosen for this study because Bingham *et al.* [11] have demonstrated that when the (^{6}Li,t) and (^{6}Li,^{3}He) reactions are studied on self-conjugate targets ($N=Z$), mirror states in the final nuclei are populated. An additional study by Bingham *et al.* [12] has shown that when the beam energy is high enough, the cross section for population of the mirror states is the same. A preliminary study using the ^{6}Li(^{6}Li,^{3}He) reaction at a beam energy of 66 MeV performed at Michigan State University [13] showed that the $\frac{1}{2}^+$ state of ^{9}Be was populated. Thus, the ^{6}Li(^{6}Li,t) reaction should populate the $\frac{1}{2}^+$ state in ^{9}B. The results of measurements on the decay of ^{9}B into the ^{8}Be + p channel are reported in the present work.

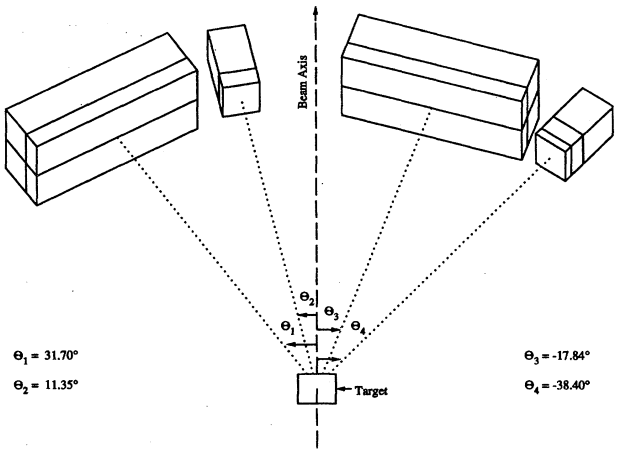

FIG. 1. Schematic of the target and detector arrangement. Each of the four detectors was placed at a distance of 10.4 cm from the target. The two ^{8}Be countertelescopes each consisted of two 1 × 5 cm strip detectors vertically separated by ≈ 2 mm, for both E and ΔE segments. The LI telescopes were comprised of E and ΔE segments each measuring 1 × 1 cm.

II. EXPERIMENTAL PROCEDURE

A 56 MeV beam of ^{6}Li was provided by the Florida State University Tandem/LINAC. A 200 μg/cm^2 ^{6}Li target made on a Formvar backing was used for the ^{9}B study. The target was transferred under vacuum to avoid oxidation. The detection system consisted of four position sensitive telescopes which were part of the CHARRISA detector array. Two of the telescopes were used to detect the alpha particles resulting from the decay of ^{8}Be, and are therefore referred to as ^{8}Be telescopes. Each of these detectors consisted of two 1 cm × 5 cm position sensitive detectors (PSD's) separated vertically by a distance of 2 mm. The ΔE segment of both these telescopes had a thickness of 224 μm, while each E segment had a thickness of 508 μm. The remaining two detectors were used to observe the protons from the decay of ^{9}B, and are referred to as light ion (LI) telescopes. Both of these telescopes were 1 cm × 1 cm in area. The LI telescope placed nearest the beam had a ΔE segment 110 μm thick and a 5000 μm thick E segment, i.e., sufficient to stop the most energetic protons. The second LI telescope set at a larger angle was designed to observe much less energetic particles and therefore consisted of a thin ΔE segment 20 μm thick followed by a second 570 μm thick ΔE and a 3000 μm thick E segment. Events were written to tape whenever any three detectors received a signal within a 100 nsec window.

The detectors were arranged such that one LI and one ^{8}Be telescope were located on a platform on each side of the beam. The detector configuration is shown in Fig. 1. All four detectors were placed at a distance of 10.4 cm from the target. The LI telescope located on the left side of the beam was set at an angle of 11.3°, and the corresponding ^{8}Be telescope was located at 31.7°. The LI telescope on the right side of the beam was set at 38.4°, and the associated ^{8}Be telescope was set at 17.8°. Each detector pair, which consists of one LI and one ^{8}Be telescope, was designed to observe a specific region of ^{9}B excitation energy. The two detector pairs, each comprised of the two detectors mounted on the same platform, were designed to have their best efficiency for observing the ground state breakup of ^{9}B and good efficiencies for observing excited states up to 3.0 MeV. Additionally, the pair formed by the LI and ^{8}Be telescopes closest to the beam had their maximum efficiencies in the region of interest, i.e., 2.0–5.0 MeV, and the last pair formed by the two detectors farthest from the beam had its best efficiency for excited states between 10 and 20 MeV.

A singles experiment was conducted using the (^{6}Li,^{3}He) reaction to populate states in ^{9}Be in order to check that the $\frac{1}{2}^+$ state was populated at the 56 MeV beam energy. These states can be explored by detecting the ^{3}He resulting from the reaction in the two LI telescopes. For this experiment the LI telescope located beam left was placed at 20 °, while the LI telescope located beam right was placed at 30°. Since the LI detectors cover ≈4° angular range, there is an appreciable kinematic shift in the energies of the detected ^{3}He for each state. However, since position information was available, it was possible to correct for the kinematic shift. The results of this process are shown in Fig. 2. As can be seen, the $\frac{1}{2}^+$ state of ^{9}Be has been populated, and from the work of Bingham *et al.* [12] we expect this reaction to also populate the $\frac{1}{2}^+$ state of ^{9}B.

The study of ^{9}B via the reaction $^6\text{Li} + {}^6\text{Li} \rightarrow {}^9\text{B} + t \rightarrow {}^8\text{Be} + p + t \rightarrow \alpha + \alpha + p + t$ requires the determination of both energy and position of the four final state particles. This kinematic completeness can be realized by detecting the two alpha particles from the decay of ^{8}Be along with the proton, and reconstructing the kinematic information associated with the undetected particle using conservation of energy and momentum. The energy and momenta of the four particles can then be used to calculate the relative velocities and relative energies between particles in the decay sequence, and with this information the excitation energy spectrum of ^{9}B can be produced. This is the RPDS

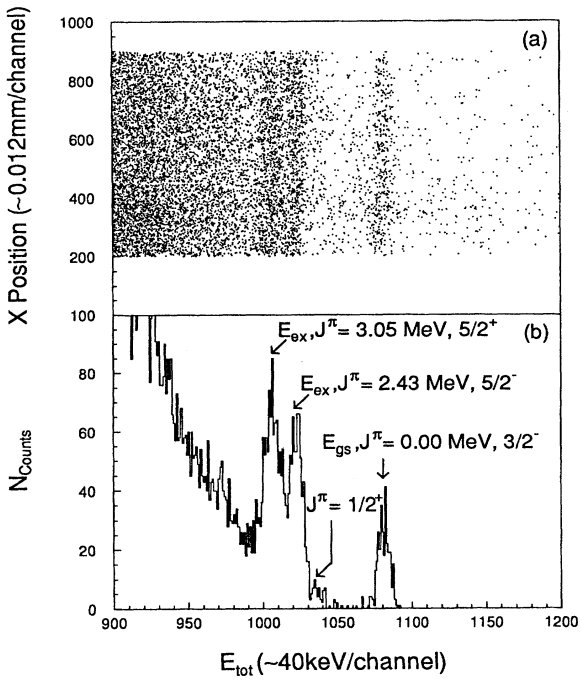

FIG. 2. (a) Scatter plot of ^{3}He energies versus position illustrating the corrections made for the kinematic shift of the ^{3}He energies over the length of LI detector number 2. (b) The projection of these events onto the energy axis which produces the ^{9}Be excitation energy spectrum from the ^{6}Li(^{6}Li,^{3}He) ^{9}Be reaction. This spectrum indicates that the $\frac{1}{2}^+$ state of ^{9}Be has been populated.

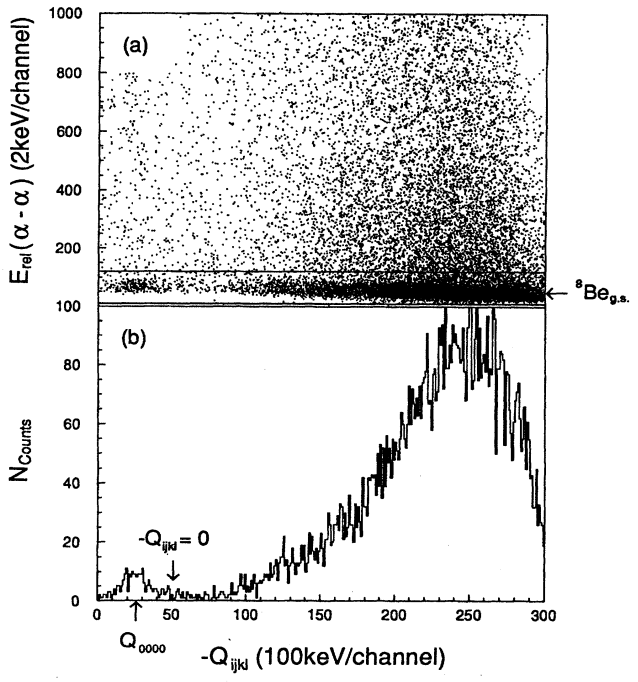

FIG. 3. (a) Plot of the four-particle negative Q value, Q_{ijkl}, from the particles detected in detector pairs 2 and 3 versus the relative energy between the two alphas detected by detector 3, $E_{rel}(\alpha$-$\alpha)$. The band in $E_{rel}(\alpha$-$\alpha)$ corresponds to events from the ground state decay of ^{8}Be. (b) Histogram of the four-particle negative Q. The peak in the $-Q_{ijkl}$ spectrum results from the four final state particles being found in their ground state, Q_{0000}.

method of Rae *et al.* [14]. The calibration of the positions and energies of these detectors is extremely important since an error in any one measurement will be propagated throughout the entire reconstruction procedure. The calibration process is further complicated by the interdependence of the energy and position signals. This interdependence causes the energy signal from equal energy particles to be somewhat different if they hit at different positions along the detector face, and similarly the position signals from particles hitting the same spot on the detector exhibit slight variations depending on the energy of the particle striking the detector.

Each segment (top and bottom) of the ^{8}Be telescopes was calibrated using alpha particles from the reaction ^{12}C(^{12}C, α) ^{20}Ne*, with ^{20}Ne in its first and second excited states at 1.63 MeV and 4.25 MeV. The ground state of ^{20}Ne was too weakly populated to provide useful calibration data. These data were taken with masks containing 25 equally spaced slits placed in front of the detector to provide position calibration signals. These masks were only used during the calibration. The angle differences between slits were determined earlier with an optical telescope, and this information was converted to distances in millimeters between the slits. Energy data were provided by the two states indicated in the above reaction for ^{12}C beam energies of 30 and 35 MeV. A linear fit of the energy centroids taken from the data to the known energy values was performed for each slit. This fit is necessary because the interdependence between the position and energy signals will cause these energy calibrations to differ slightly depending on the slit position at which they are taken. To associate the energy calibrations with the positions at which they were taken, the set of energy calibration coefficients from the linear fits undergoes a polynomial fit to an average position signal for each slit involved in the calibration. This procedure determines the energy calibration function over the whole detector. In a similar fashion, a polynomial fit of the position centroid taken from the data to the known slit positions is performed for each calibration energy. To associate the position calibrations with the energies at which these calibrations were taken, the set of coefficients from this position fit undergoes a linear fit to the average total energy centroid for each state involved in the energy calibration. This procedure gives the position calibration function for the detector.

The energy calibration for the LI telescopes was performed using proton elastic scattering from gold for five beam energies ranging from 7 to 16 MeV. The position information was provided using a mask containing five vertical and five horizontal holes arranged in a cross pattern. Unfortunately, the protons did not lose sufficient energy in the ΔE detectors to yield good position information. Therefore, a second calibration run was carried out using ^{6}Li elastic scattering from gold at 56 and 34 MeV. However, since the pulse height defect [15] will cause the energy signals from the ^{6}Li to differ slightly from those of the same energy protons, the ^{6}Li data were not suitable for the energy calibration. Thus, neither set of data contained sufficient information to provide a fit which would reflect the interdependence

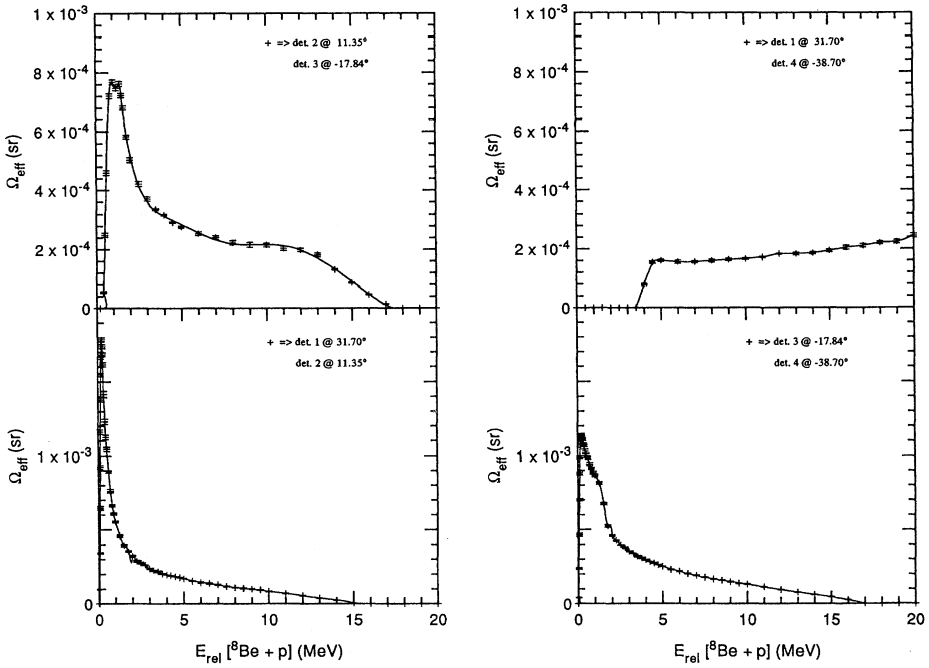

FIG. 4. The efficiency for each of the four detector pairs has been plotted as a function of the relative energy of the proton and ^{8}Be resulting from the decay of ^{9}B*. The detector angles of each pair have been given for reference.

between the position and energy signals. However, since the LI telescopes covered a limited angular range $\approx 4°$, the corrections due to the interdependence of the position and energy signals were reduced, and less rigorous calibrations sufficed. Therefore, the energy calibration was a linear fit to the proton energies, and the position calibration was a polynomial fit to the ^{6}Li slit positions.

Data reduction consisted of sorting events in time coincidence for each detector pair. Particle identification provided by the E-ΔE telescopes was used to gate the protons in the LI telescopes, and the alpha particles in the top and bottom segments of the ^{8}Be telescopes. The energy and position data for these events, along with information gathered in the calibration of the detectors, was then used to calculate relative energies, momenta, breakup angles, and Q values for each detector pair. The alpha-alpha relative energy spectrum was gated on the narrow peak resulting from the decay of the ^{8}Be ground state to ensure that the final relative energy spectrum would contain only events from the p + ^{8}Be channel. Figure 3 contains a scatter plot of the alpha-alpha relative energy versus the four-particle negative Q (Q_4), and illustrates the gate drawn on the events in the ground state ^{8}Be peak. The value of Q_4 is the mass energy in the initial system which is converted to kinetic energy of the four particles in their final state. Q_{abcd} is the value of Q_4 when each of the particles are left in a particular excited state; i.e., Q_{0101} is the value of Q_4 when particles 1 and 3 are in their ground state and particles 2 and 4 are in their first excited state. The event-by-event sort included a software gate on the ground state Q_4 peak (i.e., Q_{0000}) in order to select only those events in which all particles were emitted in their ground states.

The rigorous calibration procedure made it possible to produce α-α relative energy spectra in which the ^{8}Be ground state peak is observed with a width of 60 keV. The ground state of ^{9}B from the p + ^{8}Be relative energy spectrum was reproduced with a width of 65 keV compared to its natural width of 0.54 keV [16]. The final spectrum resolution is thus 65 keV. The ^{9}B ground state was observed to be unbound by 190 keV which is in good agreement with the accepted value of 186 keV and confirms the accuracy of the calibration and reconstruction technique.

III. ANALYSIS

A. Efficiency corrections to the relative energy spectra

The kinematics of the reaction means that the efficiency of each detector pair varies with the breakup excitation energies. Since many of the ^{9}B states have large widths, the variation of efficiency over the excitation energy of ^{9}B will distort the spectrum. In addition, the four detector pairs each have different efficiency profiles. To determine the detector efficiency over a range of ^{9}B excitation energies, a simulation of the detection system was performed using the breakup efficiency and simulation testing program BEAST [17]. The program BEAST performs a Monte Carlo simulation of the decay process using an isotropic angular distribution for the decay of each particle in the center of mass (c.m.) of its source. The effective solid angle in the c.m. of the beam and target system, Ω_{eff}, can be calculated from the results of the simulation, and the assumed isotropic angular distribution means that Ω_{eff} is proportional to the probability of detecting particles from a given decay sequence in a coincidence measurement.

The efficiencies were calculated for a number of points throughout a ^{9}B relative energy range from 0 to 25 MeV to make the efficiency corrections to the relative energy spectra. Particular attention was paid to the relative energy range of interest from 0 to 5 MeV. In the simulation it was necessary to use 10^8 total events to provide 1000 events in the relative energies of interest, which gives an error under 5% in that region. Figure 4 shows a plot of the effective solid angle

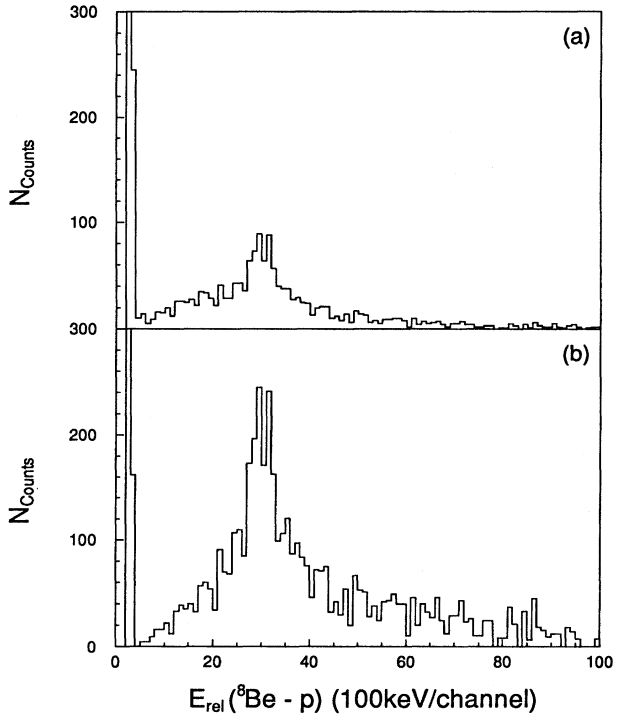

FIG. 5. (a) The summed ^{8}Be+p raw relative energy spectra for all four detector pairs. (b) The summed efficiency corrected ^{8}Be+p relative energy spectrum. The two spectra have been normalized such that their ground state ^{9}B peaks have the same height.

versus the ^{8}Be + p relative energy for the four detector configurations used in this measurement. Figure 4 also displays a polynomial fit to the calculated efficiencies denoted by the solid line in these plots. Because of the difficulty in fitting the entire curve at once, each efficiency curve was divided into two or three sections, and the fits were performed on each of these sections. These efficiencies were then used to correct the raw relative energy spectra for each of the four detector combinations. The corrected relative energy spectra were then summed, to produce the composite relative energy spectrum in Fig. 5. The summed raw ^{8}Be + p relative energy spectrum is shown in Fig. 5 for comparison. One should also note that the $\frac{5}{2}^-$ state which decays via the ^{5}Li + α channel does not appear in this ^{8}Be + p relative energy spectrum.

B. Line shape analysis

The determination of states populated in the final ^{9}B spectrum requires a multiple-level analysis of this spectrum. Fitting these states with Gaussian or Breit-Wigner line shapes is unacceptable due to the close proximity of the threshold energy for the formation of ^{8}Be + p. To produce line shapes with the correct threshold energy dependence, the one-level approximation of Lane and Thomas [18] for a three-body disintegration treated as a succession of two-body disintegrations was chosen to model the decay process.

The method of Lane and Thomas [18] assumes that these reactions have the form $a + b \rightarrow c + (d \rightarrow e + f)$, where the initial particles form a resonance in the compound nuclear system $(a + b)$ which then decays into particles c and d, after which particle d decays into particles e and f. However, the reaction under consideration is of the form ^{6}Li + ^{6}Li $\rightarrow t$ + [^{9}B $\rightarrow p$ + (^{8}Be $\rightarrow \alpha + \alpha$)]; thus the first resonance occurs presumably after a direct reaction creates a state which is unbound to particle decay, and therefore this represents a different formation mechanism of the initial resonance. The formation factors that appear in the discussion of Lane and Thomas are not applicable to this situation, and those terms which apply to the formation factor of the state have been included into a normalization factor for each state, N, which is treated as a free parameter in this analysis.

The one-level approximation requires that the total cross section for the reaction be known. In the present case, the extremely low coincidence count rate meant that a full angular distribution measurement of decay particles was impractical, and therefore the spectrum being fit represents simply a cross section averaged over the angles covered by the detectors. The effect of this on the fitting of the $\frac{1}{2}^+$ or $\frac{1}{2}^-$ state should be small since they decay isotropically. The $\frac{5}{2}^+$ state will not decay isotropically, but lack of information again forces us to assume that the difference between the observed and total cross section for this state will be small. The differential cross section under the conditions outlined above is given by

$$\frac{d\sigma}{dE_c} = \frac{N\Gamma_{\lambda c}}{(E_\lambda + \Delta_{\lambda c} - E_c)^2 + \frac{1}{4}\Gamma_\lambda^2}, \tag{1}$$

where E_λ is the energy of the resonance, and E_c is the relative energy between the particles which form the resonant state. $\Gamma_{\lambda c}$ is the partial width of the resonant state in channel c, Γ_λ is the total width of the resonant state, and $\Delta_{\lambda c}$ is the partial shift of the resonant state in channel c. The subscript c refers to the decay channel, in this case the ^{8}Be+p channel.

The partial width $\Gamma_{\lambda c}$ and corresponding partial shift $\Delta_{\lambda c}$ for the channel under consideration are given in terms of the reduced widths $\gamma_{\lambda c}^2$, the penetration factors P_c, and the shift functions S_c as [18]

$$\Gamma_{\lambda c} = 2P_c\gamma_{\lambda c}^2 \tag{2}$$

and

$$\Delta_{\lambda c} = -(S_c - B_c)\gamma_{\lambda c}^2, \tag{3}$$

where B_c is a logarithmic derivative quantity which is involved in the specification of the boundary conditions to be satisfied. The penetration and shift factors result from matching the logarithmic derivative at the boundary r_c, and can be defined [18] in terms of regular and irregular solutions to the Coulomb wave equation F and G as

$$P_c = \left[\frac{\rho_c}{(F_c^2 + G_c^2)}\right]_{r=r_c}, \quad S = \left[\frac{\rho(FF' - GG')}{(F^2 + G^2)}\right]_{r=r_c}, \tag{4}$$

where ρ is the interaction radius. The Coulomb wave functions were obtained from an algorithm developed by Steed and presented by Barnett *et al.* [19]. This algorithm has been incorporated into the computer program used to calculate the line shapes, and requires the knowledge of the interaction radius, $\rho_c = k_c r_c$, the angular momentum L, and the Coulomb field parameter η_c which is given by

$$\eta_c = \frac{M_c Z_1 Z_2 e^2}{\hbar^2 k_c}, \tag{5}$$

where M_c is the reduced mass of the two particles in channel c, and Z_1 and Z_2 are the atomic numbers of these two particles. The wave number k_c is given by

$$k_c = \sqrt{\frac{2M_c|E_c|}{\hbar^2}}. \tag{6}$$

For the three levels considered here in ^{9}B ($J^\pi = \frac{1}{2}^+$, $\frac{1}{2}^-$, $\frac{5}{2}^+$), the $p + {}^8\mathrm{Be}_{\mathrm{g.s.}}$ channel appears to be the only significant open channel. For the $\frac{5}{2}^+$ state this is known from earlier work [10,16]. For the $\frac{1}{2}^-$ level the mirror nucleus is known to decay only into $n + {}^8\mathrm{Be}_{\mathrm{g.s.}}$. The $\frac{1}{2}^+$ state decay in the energy range considered here is expected to occur via the $p + {}^8\mathrm{Be}_{\mathrm{g.s.}}$ channel. This conclusion is based on the fact that the $^5\mathrm{Li} + \alpha$ channel can only become significant at higher energies since the $^5\mathrm{Li} + \alpha$ decay threshold in ^{9}B is at 1.69 MeV and the decay of this state into this channel must be p wave. Consequently, we have $\Gamma_\lambda = \Gamma_{\lambda c}$, $\Delta_\lambda = \Delta_{\lambda c}$, and subsume the constant level shift into the definition of the resonance energy E_λ. In accordance with the usual definitions of analog states we choose B_c for the $p + {}^8\mathrm{Be}_{\mathrm{g.s.}}$ to be the logarithmic derivative in the parent channel $n + {}^8\mathrm{Be}_{\mathrm{g.s.}}$, i.e.,

$$B_p = S_n(E_n), \tag{7}$$

in which E_n is the energy of the neutron in the mirror ^{9}Be state. Because of the close proximity of the $p + {}^8\mathrm{Be}_{\mathrm{g.s.}}$ threshold to the states in ^{9}B, the energy dependence of the penetration and shift functions plays an important role in describing the low energy regime, particularly for the $\frac{1}{2}^+$ state.

The one-level approximation assumes that the resonance under consideration is well removed from other states which may interfere. However, the states under consideration here will have considerable overlap due to their proximity in excitation energy and large widths. Therefore, an additional interference term was included to model the effects of the overlapping resonances in this region. The form of the interference term $d\sigma_{i,j}/dE_c$ between states i and j, in which both nuclei have one open decay channel c, is given by

$$\frac{d\sigma_{i,j}}{dE_c} = N_{i,j}\sqrt{\Gamma_{\lambda_i c}\Gamma_{\lambda_j c}}\,2\mathrm{Re}\left\{ \frac{e^{i\phi_{i,j}}}{\left[(E_{\lambda_i}+\Delta_{\lambda_i}-E_c)-\frac{i}{2}\Gamma_{\lambda_i}\right]\left[(E_{\lambda_j}+\Delta_{\lambda_j}-E_c)+\frac{i}{2}\Gamma_{\lambda_j}\right]} \right\}. \tag{8}$$

In the present case the open channel is $^8\mathrm{Be} + p$. The information on the strength of the interference term is contained in the variable $N_{i,j}$, and the phase of the interference is given by $\phi_{i,j}$.

Taking only the real part of the above equation yields the following form of the interference term used in fitting the line shapes:

$$\frac{d\sigma_{i,j}}{dE_c} = 2N_{i,j}\sqrt{\Gamma_{\lambda_i c}\Gamma_{\lambda_j c}}\left\{ \frac{[(E_{\lambda_i}+\Delta_{\lambda_i}-E_c)(E_{\lambda_j}+\Delta_{\lambda_j}-E_c)+\frac{1}{4}\Gamma_{\lambda_i}\Gamma_{\lambda_j}]\cos(\phi_{i,j})}{[(E_{\lambda_i}+\Delta_{\lambda_i}-E_c)^2+\frac{1}{4}\Gamma_{\lambda_i}^2][(E_{\lambda_j}+\Delta_{\lambda_j}-E_c)^2+\frac{1}{4}\Gamma_{\lambda_j}^2]} \right.$$
$$\left. + \frac{[\frac{1}{2}\Gamma_{\lambda_j}(E_{\lambda_j}+\Delta_{\lambda_j}-E_c)-\frac{1}{2}\Gamma_{\lambda_i}(E_{\lambda_i}+\Delta_{\lambda_i}-E_c)]\sin(\phi_{i,j})}{[(E_{\lambda_i}+\Delta_{\lambda_i}-E_c)^2+\frac{1}{4}\Gamma_{\lambda_i}^2][(E_{\lambda_j}+\Delta_{\lambda_j}-E_c)^2+\frac{1}{4}\Gamma_{\lambda_j}^2]} \right\}. \tag{9}$$

These equations were included in the program LINESHAPE, which was designed to find the best description of the experimental spectrum using the resonance energy, formation factor, and reduced width of each state along with the two parameters governing the interference effects between each pair of states, the interference strength, and phase. A two-state fit has 8 parameters and a three-state fit requires 15. The simplex minimization method of Nelder and Mead [20] was used to find the theoretical line shape which best describes the data. This simplex minimization method compares the value of the function at $n + 1$ vertices, and replaces the vertex which corresponds to the highest value of the function being minimized with another point. This process continues until the vertices contract on the final minimum. The χ^2 function, in this case, is formed from the calculated and observed line shapes and the statistical error in the observed line shape (i.e., $\sigma_i = \sqrt{N_i}$) and has the form

$$\chi^2 = \sum_i \left\{ \frac{\left[\frac{d\sigma_i}{dE_c}(x) - \frac{d\sigma_i}{dE_c}(\mathrm{obs})\right]}{\sigma_i(\mathrm{obs})} \right\}^2. \tag{10}$$

The Hessian or error matrix is calculated using finite differences. That is, the full matrix of second derivatives of the

function with respect to the variable parameters is calculated and inverted to produce the error matrix.

C. Discussion of the line shape analyses

The known energy levels in ^{9}B below 4.0 MeV are the $\frac{3}{2}^-$ ground state with a width of 0.54 keV, the $\frac{5}{2}^-$ state at 2.36 MeV with a width of 81 keV, and the $\frac{5}{2}^+$ state at 2.78 MeV with a width of 550 keV [16]. In addition, the $\frac{1}{2}^-$ state of ^{9}B has also been observed recently at 2.83 MeV with a width of 3.1 MeV by Pugh [5], using the ^{9}Be(p,n) reaction. The $\frac{5}{2}^-$ state at 2.36 MeV is not included in this analysis since our spectrum gives little indication of its presence and it has been observed to have a decay branch via $p+{}^8$Be less than $\approx 0.5\%$ [10]. Additionally, if this small branching ratio leads to a significant contribution to the $p+{}^8$Be line shape, it will appear all in one channel bin since the $\frac{5}{2}^-$ width is 70 keV. Note that when the decay proceeds through the $p+{}^8$Be resonance, there is no noticeable increase in the width of the state from the ^{8}Be ground state since it has a width on the order of 10 eV.

In order to learn as much from the data as possible, a number of line shape analyses was performed. The first fit used two states and included interference effects to see if the data could be fit with only the known $\frac{5}{2}^+$ [16] and the recently observed $\frac{1}{2}^-$ [5] states. This test is designed to see if the $\frac{1}{2}^+$ state is needed to describe the data. Next, a two-state fit of the $\frac{1}{2}^+$ and $\frac{5}{2}^+$ states including interference effects is utilized to check the strength of the contribution of the $\frac{1}{2}^-$ state. Last, two separate three-state fits without interference effects were conducted. The first was designed to set an absolute lower limit on the $\frac{1}{2}^+$ excitation energy consistent with the data, while the second was used to obtain a best fit value of the excitation energy of the first excited state of ^{9}B for comparison with other experiments in which the interference effects have been ignored. A three-state fit with interference was not performed since it would require a minimum of ten free parameters, and the present data are not sufficient to allow the determination of this many parameters.

1. Two-state line shape analysis using the $\frac{1}{2}^-$ and $\frac{5}{2}^+$ states

The first step in the analysis is to determine whether the $\frac{1}{2}^+$ state is present. To do this, the two states which have been observed in this energy region ($\frac{5}{2}^+$, 2.79 MeV [16] and $\frac{1}{2}^-$, 2.83 MeV [5]) are included in a fit which will determine if the ^{9}B spectrum reconstructed from $p+{}^8$Be events can be described without including the $\frac{1}{2}^+$ state. Since the energy of the $\frac{5}{2}^+$ state is well known, we are able to fix its energy in the fitting process. The reduced width of this state is unknown and so it is taken from its mirror ^{9}Be, since the boundary conditions which lead to the reduced widths should be similar. This works well for the $\frac{5}{2}^+$ state of ^{9}B since the reduced width taken from the ^{9}Be data in Ajzenberg-Selove's compilation [16], $\gamma_c^2=1.79$ MeV, using an r_c of 4.35 fm, produces a calculated width approximately equal to the 550 keV reported width in ^{9}B. Since the properties of the $\frac{1}{2}^-$ state are not well established, the energy and reduced width of this state are left as free parameters. Therefore, there are six parameters involved in fitting the line shape,

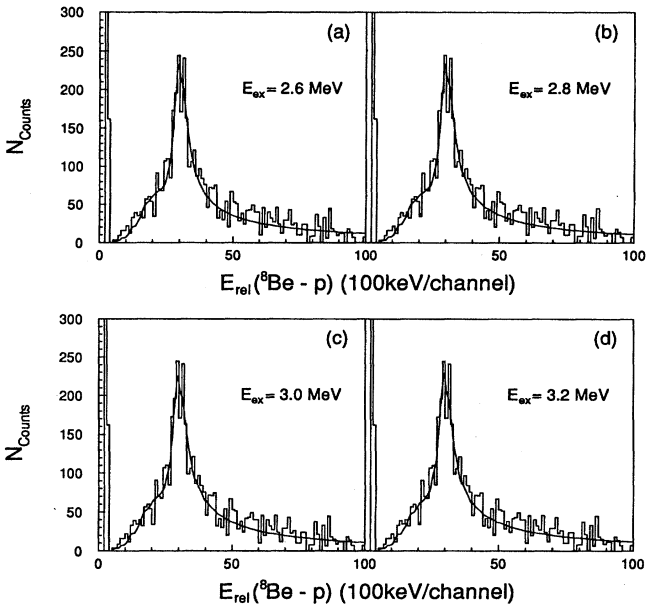

FIG. 6. For the two-state analysis using the $\frac{1}{2}^-$ and $\frac{5}{2}^+$ states, the efficiency corrected ^{8}Be$+p$ relative energy spectrum is plotted along with its calculated line shape denoted by the solid curves for four excitation energies of the $\frac{1}{2}^-$ state ranging from 2.6 to 3.2 MeV. The ^{9}B excitation energy is related to this relative energy via $E_{ex}=E_{rel}-0.185$ MeV.

namely, the formation factors of both states, the energy and reduced width of the $\frac{1}{2}^-$ state, and the strength and phase of the interference between these two states. To reduce the number of parameters varied in each fit to 5, the excitation energy of the $\frac{1}{2}^-$ state was held fixed in each fit, and the fit was performed over a range of $\frac{1}{2}^-$ relative energies ranging from 2.5 to 3.4 MeV in 0.1 MeV steps (this corresponds to an excitation energy range of 2.31–3.21 MeV). The data in the relative energy range from 0.6 to 4.0 MeV were included in the fit. Data above 4.0 MeV were not included due to both poor statistics, which are exaggerated in the efficiency correction routine, and the introduction of contributions from states lying above 4 MeV.

Figure 6 shows the results of the fit for selected $\frac{1}{2}^-$ excitation energies. Each of these plots shows that the calculated line shape underpredicts the observed line shape at energies below $\approx$ 1.5 MeV because the calculated line shape has the wrong inflection at these low energies. Thus, attempting to fit the observed line shape with only the $\frac{1}{2}^-$ and $\frac{5}{2}^+$ states cannot account for all the data below 1.5 MeV. Table I shows the results of the fitting procedure for each of the $\frac{1}{2}^-$ excitation energies fit, as well as the full width at half maximum (FWHM) of the $\frac{1}{2}^-$ state. While χ^2 is essentially a constant over the energy region scanned, perhaps fortuitously, the minimum χ^2 results in an excitation energy of 2.91 MeV and a width of 3.03 MeV, which agrees remarkable well with Pugh's findings [5] of a 2.83 MeV excitation energy and a 3.12 MeV width. For this case, the difference between the observed and calculated line shape is illustrated in Fig. 7. This difference shows the unaccounted for excess counts below $\approx$ 1.5 MeV. It should be noted that the calculated fit

TABLE I. Parameters involved in fitting the $\frac{1}{2}^-$ and $\frac{5}{2}^+$ states in ^{9}B.

	$\frac{1}{2}^-$ state			$\frac{5}{2}^+$ state	interference terms		
E_{ex} (MeV)	γ^2 (MeV)	Γ (MeV)	N	N	N_I	ϕ_I (deg)	χ^2
2.31	5.34	2.18	96.8	58.1	177.8	-135.8	5.35
2.41	3.94	2.20	81.7	51.0	104.4	-126.5	5.35
2.51	4.75	2.42	108.5	64.1	238.4	-148.3	5.26
2.61	4.83	2.57	124.6	71.3	317.3	-154.9	5.23
2.71	4.75	2.71	126.3	67.2	284.7	-157.8	5.22
2.81	4.77	2.86	143.8	72.4	356.7	-162.3	5.20
2.91	5.37	3.05	161.3	76.3	432.9	-166.4	5.17
3.01	5.90	3.22	164.6	71.0	398.6	-169.6	5.20
3.11	6.27	3.38	162.7	66.0	344.0	-172.3	5.32
3.21	4.64	3.44	167.4	73.5	385.0	-176.8	5.28

represents the maximum contribution to the spectrum that can be produced in the low energy region from the $\frac{1}{2}^-$ and $\frac{5}{2}^+$ states permitted by the data and so the excess counts will in fact increase with any changes in the fitting parameters. This again indicates that a third state must be present to account for these events.

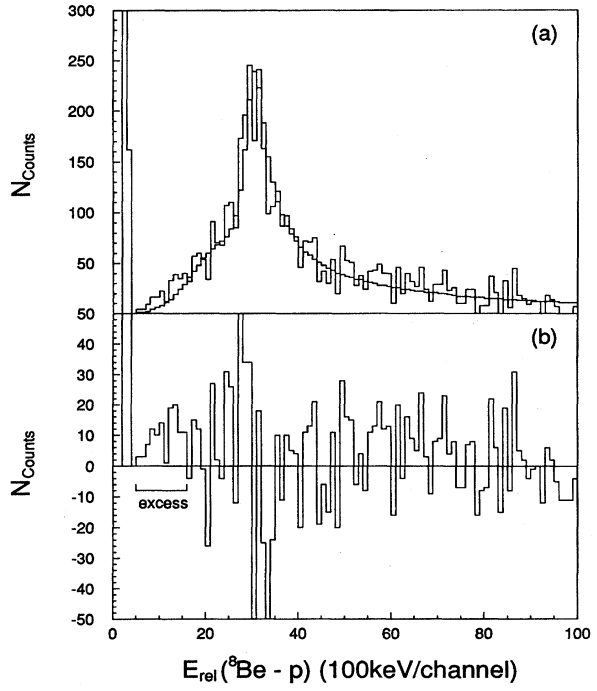

FIG. 7. (a) The efficiency corrected ^{8}Be+p relative energy spectrum is plotted along with its calculated line shape from the $\frac{1}{2}^-$ and $\frac{5}{2}^+$ line shape analysis denoted by the solid curve (plotted in histogram form to show exact counts since the fitting routine uses a spline routine to draw the smooth curve). The ^{9}B excitation energy is related to this relative energy via $E_{ex} = E_{rel} - 0.185$ MeV. (b) The difference between the calculated line shape, and the experimental data showing the region in which the excess counts were observed.

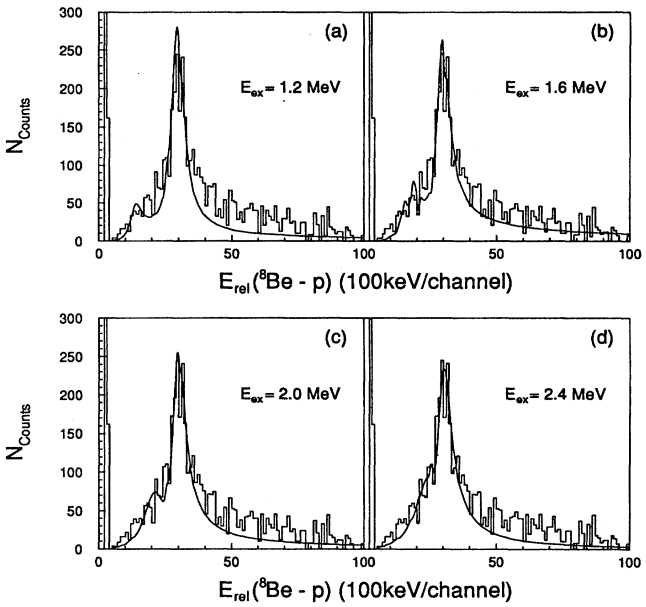

FIG. 8. For the two-state analysis using the $\frac{1}{2}^+$ and $\frac{5}{2}^+$ states, the efficiency corrected ^{8}Be+p relative energy spectrum is plotted along with its calculated line shape denoted by the solid curves for four excitation energies of the $\frac{1}{2}^+$ state ranging from 1.2 to 2.4 MeV. The ^{9}B excitation energy is related to this relative energy via $E_{ex} = E_{rel} - 0.185$ MeV.

2. *Two-state line shape analysis using the $\frac{1}{2}^+$ and $\frac{5}{2}^+$ states*

A second two-state fit using the assumed $\frac{1}{2}^+$ and known $\frac{5}{2}^+$ states and including interference between them was executed to gauge the extent of the contribution of the $\frac{1}{2}^-$ state to the data. The energy and reduced width of the $\frac{5}{2}^+$ state are again set to the values reported in the previous section. The reduced width of the $\frac{1}{2}^+$ state was set to the value found in the mirror nucleus ^{9}Be where $\gamma^2 = 0.5$ MeV [21]. This reduces the number of free parameters to 5. As before, the range of the fit was limited to the region between 0.5 and 4.0 MeV, since contributions from other states can become significant outside this region. A series of fits was performed varying the $\frac{1}{2}^+$ excitation energy from 1.0 to 2.6 MeV using step sizes of 200 keV to examine the range of $\frac{1}{2}^+$ excitation energies over which adequate descriptions of the data could be obtained.

The results for four selected values among the range of excitation energies studied are presented in Fig. 8, and Table II gives the values of the parameters used in the description of the data for each excitation energy in the above range. The best two-state fit occurs at the $\frac{1}{2}^+$ excitation energy of 1.6 $\pm$0.1 MeV which is in the region where other works have claimed to observe this state [2,22,23]. The previous section shows that the regions where the present fits are poorest, i.e., the high energy tail between 3.0 and 4.0 MeV and the region between 1.5 and 2.5 MeV, are precisely the regions that the $\frac{1}{2}^-$ state fits well. This indicates that the $\frac{1}{2}^-$ state must be present to adequately describe the data. This result, along with the previous attempt to fit the data without the $\frac{1}{2}^+$ state, indicates that the $\frac{1}{2}^+$, $\frac{5}{2}^+$, and $\frac{1}{2}^-$ states are all present in this

TABLE II. Parameters involved in fitting the $\frac{1}{2}^+$ and $\frac{5}{2}^+$ states in ^{9}B.

	$\frac{1}{2}^+$ state		$\frac{5}{2}^+$ state interference terms			
E_{ex} (MeV)	Γ (MeV)	N	N	N_I	ϕ_I (deg)	χ^2
1.00	0.49	53.9	216.6	514.6	115.0	10.5
1.20	0.59	11.1	71.5	41.2	139.4	10.5
1.40	0.69	10.2	61.1	10.7	163.7	9.51
1.60	0.77	80.6	199.4	344.6	122.5	7.04
1.80	0.85	13.1	52.9	13.1	1.4	7.95
2.00	0.93	18.3	53.4	19.2	42.5	7.59
2.20	1.00	12.4	31.8	43.0	6.1	7.28
2.40	1.07	6.4	4.7	73.1	8.6	7.15
2.60	1.14	26.8	1.3	56.6	35.7	7.50

energy region. A consequence of this conclusion is that the $\frac{1}{2}^-$ state must have a $p+{}^8$Be decay branch.

3. *Three-state line shape analysis without interference terms*

There have been many previous attempts to find and measure the excitation energy of the first excited $\frac{1}{2}^+$ state of ^{9}B [1–3,22–26]. Table III lists the results from a number of these experiments. One common factor in all these works is the absence of interference terms between levels when performing the fit to the measured line shapes to determine their excitation energies. Thus, to get a number to compare with these previous results, a three-state fit without interference terms was performed. The results of this fit can also be used to set a lower limit on the $\frac{1}{2}^+$ excitation energy. This can be accomplished because the interference effects are reduced at low excitation energies because the $\frac{5}{2}^+$ state has almost no contribution below 1.5 MeV, and while the $\frac{1}{2}^-$ state has a noticeable contribution down to $\approx$1.0 MeV, the interference term will have its smallest effect at the energy of interest here (i.e., the minimum possible energy of the $\frac{1}{2}^+$ state). For this fit, the reduced width and excitation energy of the $\frac{5}{2}^+$ state were fixed at their known values (see Sec. III C 1). Since our results in Sec. III C 1 agreed well with those of Pugh [5], the excitation energy of the $\frac{1}{2}^-$ state was fixed to Pugh's value of 2.83 MeV, and the reduced width was set to a value (γ^2=7.5 MeV) that reproduced its reported $\approx$ 3.0 MeV width. The reduced width of the $\frac{1}{2}^+$ state was again set to its value found in its mirror ^{9}Be, i.e., γ^2 = 0.5 MeV. The

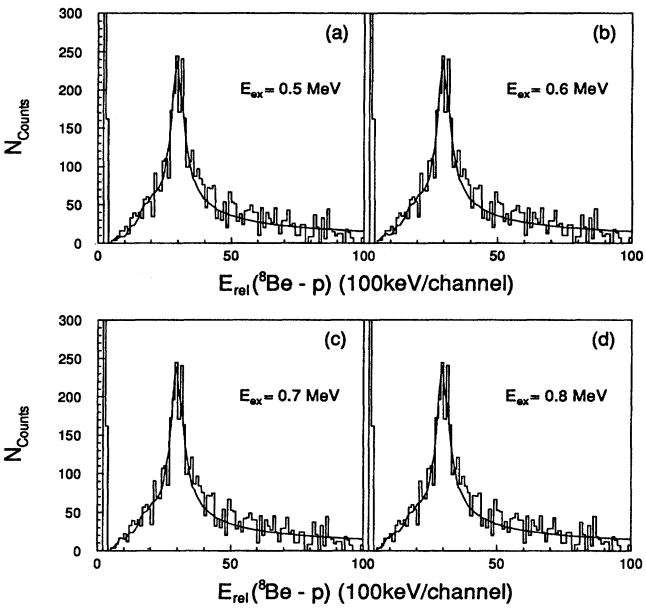

FIG. 9. The efficiency corrected ^{8}Be+p relative energy spectrum is plotted along with its calculated line shape from the three-state fit denoted by the solid curve for four excitation energies of the $\frac{1}{2}^+$ state ranging from 0.5 to 0.8 MeV. The ^{9}B excitation energy is related to this relative energy via $E_{ex} = E_{rel} - 0.185$ MeV. Channel numbers above 40 were not included in the fitting procedure.

fit was conducted for excitation energies ranging from 0.5 to 2.0 MeV in 0.1 MeV steps to observe how the fit varies with $\frac{1}{2}^+$ excitation energy. This resulted in only three free parameters, namely, the normalizations of the states.

The results of the three-state analysis are displayed in Fig. 9 for four energies of the $\frac{1}{2}^+$ state ranging from 0.5 to 0.8 MeV. If the $\frac{1}{2}^+$ state is placed at an energy at or below 0.6 MeV, the low energy counts are overpredicted; thus 0.6 MeV is the lowest possible energy at which the $\frac{1}{2}^+$ state can occur. The three-state fit parameters are given in Table IV, along with the width of the $\frac{1}{2}^+$ state. The best fit energy was found to be 0.73 MeV $\pm$ 0.05 MeV which agrees well with the 900 keV prediction of Sherr and Bertsch. Figure 10 shows the best fit calculation and displays the contributions from each individual state. From this figure, it can be seen that the $\frac{1}{2}^+$ state has a small but vital contribution in describing the line-

TABLE III. Comparison of the present results with previous works which measured the $\frac{1}{2}^+$ excitation energy.

Author	Reaction	E (MeV)	Γ (MeV)
Present work	^{6}Li(^{6}Li,t)	1.6 $\pm$ 0.1	0.77
Marion *et al.* [24]	^{9}Be(p,n)	1.4	$\approx$ 1.0
Kroepfl and Browne [22]	^{10}B(^{3}He,α)	1.58	0.71
Slobodrian *et al.* [25]	^{9}Be(p,n)	1.40	-
Symons and Treacy [23]	^{12}C(p,α)	1.7 $\pm$ 0.2	γ^2 = 1.0
Barker and Treacy [26]	^{10}B(^{3}He,α)	1.2	γ^2 = 1.0
Kadija *et al.* [1]	^{9}Be(^{3}He,t)	1.16 $\pm$ 0.05	γ^2 = 1.08 $\pm$ 0.05
Arena *et al.* [2]	^{10}B(^{3}He,α)	1.8 $\pm$ 0.2	0.9 $\pm$ 0.3
Burlein *et al.* [3]	^{9}Be(^{6}Li,^{6}He)	1.32 $\pm$ 0.08	0.86 $\pm$ 0.26

TABLE IV. Parameters involved in fitting the $\frac{1}{2}^+$, $\frac{1}{2}^-$, and $\frac{5}{2}^+$ states in ^{9}B.

	$\frac{1}{2}^+$ state		$\frac{5}{2}^+$ state	$\frac{1}{2}^-$ state	
E_{ex} (MeV)	Γ (MeV)	N	N	N	χ^2
0.50	0.22	0.28	41.1	140.0	4.63
0.60	0.28	0.59	41.7	137.1	4.44
0.70	0.33	1.00	41.8	134.4	4.26
0.80	0.38	1.12	42.2	132.1	4.28
0.90	0.44	1.18	42.4	130.1	4.42
1.00	0.49	1.12	42.4	130.5	4.53
1.10	0.54	1.35	42.7	128.6	4.54
1.20	0.59	1.58	42.8	126.4	4.55
1.30	0.64	1.60	42.7	126.3	4.63
1.40	0.69	1.19	42.3	129.8	4.74
1.50	0.73	0.21	41.0	139.5	4.83

shape below 1.5 MeV. These results also indicate that the excitation energy of the $\frac{1}{2}^+$ state is below 1.67 MeV, the difference in energy between the ground and first excited state in ^{9}Be, and therefore the Thomas-Ehrman shift is normal for the mass 9 system.

D. Comparison with earlier works

Table III lists the results from a number of works which have attempted to identify the excitation energy of the $\frac{1}{2}^+$ state. For comparison, we have included our value from the two-state fit with interference in the table since only one work presented here included the $\frac{1}{2}^-$ state in their calculations. Many of the early experiments which reported observing the $\frac{1}{2}^+$ state [22,24,25] suffered from large backgrounds, a problem which has been largely removed in the present experiment. Also, when peak fits were attempted [22], Breit-Wigner line shapes were used, which lack the high energy tails necessary to describe peaks near threshold, whereas the present work used Lorentzian line shapes. In addition, these experiments populated both the $\frac{5}{2}^-$ and $\frac{5}{2}^+$ states at 2.36 MeV and 2.79 MeV, making the experimental spectrum considerably more complex than the present one. The results presented in these early papers (from 1.4 to 1.6 MeV) agree well with our value of 1.6 MeV from the two-state fit with interference. A view expressed by many of the authors in their works is that the differences are largely due to the difficulty in interpreting the experimental spectra. The first works to use more sophisticated analyses were carried out by Symons and Treacy [23], and later by Barker and Treacy [26]. Their analyses are both based on an R matrix formalism almost identical to the one employed here. However, the data sets available for their works had large backgrounds which had to be subtracted before the data could be analyzed, and their experimental spectra also had contributions from the $\frac{5}{2}^-$ state, which probably was the reason for the high $\frac{1}{2}^+$ excitation energy of 1.7 MeV reported by Symons and Treacy [23]. The later result of Barker and Treacy [26] placed the $\frac{1}{2}^+$ state at 1.2 MeV. The results of more recent works are plagued by similar problems. Kadija *et al.* [1] found the excitation energy of the $\frac{1}{2}^+$ state to be 1.16 MeV with a width of 1.08 MeV. The line shapes used to fit the data were similar to our own; however, Kadija *et al.* had to strip off the breakup contributions to their data using a complicated process before they arrived at a line shape. Arena *et al.* [2] performed a coincidence experiment in which alphas and protons resulting from the decay of ^{9}B were detected; however, they did not have enough information to reconstruct the events as was done here, and had to resort to a more complicated analysis to separate out the ^{8}Be + p channel. The resulting excitation energy of the $\frac{1}{2}^+$ state was 1.8 MeV, with a width of 0.8 MeV. The slight discrepancy compared to our result of 1.6 MeV in the two-state fit with interference may be due to their method of isolating the p + ^{8}Be channel. Burlein *et al.* [3] also used a similar fitting technique with Lorentzian line shapes, but they had to also fit the $\frac{5}{2}^-$ state which is not present in our spectrum, and they had to assume a quadratic background, which was not necessary here. Burlein *et al.* [3] performed two fits: one with the 2.83 MeV $\frac{1}{2}^-$ state but without the 2.79 MeV $\frac{5}{2}^+$ state, and one with the 2.79 MeV $\frac{5}{2}^+$ state, and a state at 3.5 MeV. The value for the fit of Burlein *et al.* using the $\frac{5}{2}^+$ and $\frac{1}{2}^+$ state without interference (1.32 MeV) is 300 keV lower than our value of 1.6 MeV using an interference term, and the fit of Burlein *et al.* using the $\frac{1}{2}^+$ and $\frac{1}{2}^-$ states (1.16 MeV) is about 400 keV higher than our result from the three-state fit without interference. However, another ^{9}Be(^{6}Li, ^{6}He) work [4] does not show the structure in the spectrum observed by Burlein *et al.*, which only adds to the confusion of the location of the $\frac{1}{2}^+$ state.

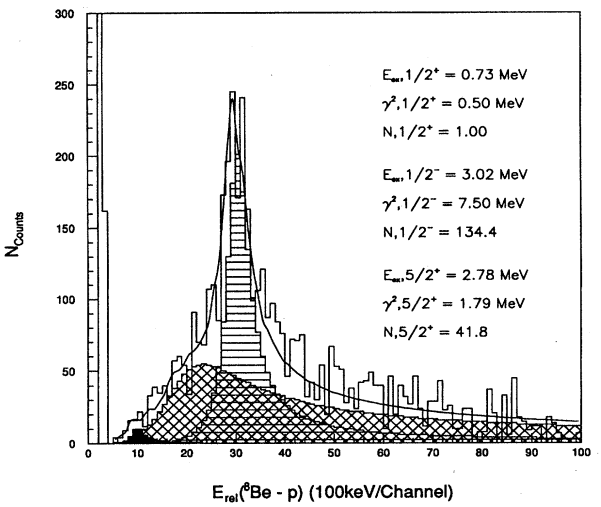

FIG. 10. The efficiency corrected ^{8}Be+p relative energy spectrum is plotted along with its calculated line shape from the three-state fit denoted by the shaded curve. The individual contributions from each state to the total line shape are shown by the solid data for the $\frac{1}{2}^+$ state, cross-hatched lines for the $\frac{1}{2}^-$ state, and horizontal lines for the $\frac{5}{2}^+$ state. The ^{9}B excitation energy is related to this relative energy via $E_{ex} = E_{rel} - 0.185$ MeV. Channel numbers up to 40 were included in the fitting procedure.

IV. CONCLUSION

In summary, the first excited state of ^{9}B has been observed at an energy $\geq$ 0.60 MeV in the ^{8}Be + p reaction

channel using the reaction ^{6}Li(^{6}Li,t)^{9}B at a laboratory beam energy of 56 MeV. The observation of this state was made possible through the use of the RPDS method which provided low background, and allowed the removal of the strongly populated $\frac{5}{2}^-$ state of ^{9}B which decays exclusively via the ^{5}Li + α channel. A two-state fit to the observed spectrum with interference effects yielded an excitation energy of the $\frac{1}{2}^+$ state of 1.6±0.1 MeV. This value of the excitation energy corresponds to a normal Thomas-Ehrman shift in the mass 9 system. In addition, the $\frac{1}{2}^-$ state of ^{9}B was observed to decay via the ^{8}Be+p reaction channel.

The results presented for all studies of ^{9}B to date suffer from the same problems as encountered here. The extracted excitation energy of the $\frac{1}{2}^+$ state depends crucially on being able to include level interference terms in the fitting procedure. While the present experiment has provided the cleanest spectrum to date, one would need a great deal more data at numerous angles before a proper analysis can be carried out.

ACKNOWLEDGMENTS

The authors would like to thank Dr. Paul Beaumont and Dr. Harrison Prosper for their aid with the statistical analysis presented here. This work was supported in part by the National Science Foundation, the State of Florida, and the SERC (U.K.).

[1] K. Kadija, G. Paić, B. Antolković, A. Djaloeis, and J. Bojowald, Phys. Rev. C **36**, 1269 (1987).
[2] N. Arena, S. Cavallaro, G. Fazio, G. Giardina, A. Italiano, and F. Mezzanares, Europhys. Lett. **5**, 517 (1988).
[3] M. Burlein, H.T. Fortune, P.H. Kutt, R. Gilman, R. Sherr, and J.D. Brown, Phys. Rev. C **38**, 2078 (1988).
[4] W.N. Catford, L.K. Fifield, E.L. Reber, K.W. Kemper, and J.D. Brown, Nucl. Phys. **A550**, 517 (1992).
[5] B. Pugh, Ph.D. dissertation, MIT, 1985.
[6] R. Sherr and G. Bertsch, Phys. Rev. C **32**, 1809 (1985).
[7] R.G. Thomas, Phys. Rev. **88**, 1109 (1952).
[8] J.B. Ehrman, Phys. Rev. **81**, 412 (1951).
[9] F.C. Barker, Aust. J. Phys. **40**, 307 (1987).
[10] D.H. Wilkinson, J.T. Sample, and D.E. Alburger, Phys. Rev. **146**, 662 (1966).
[11] H.G. Bingham, H.T. Fortune, J.D. Garrett, and R. Middleton, Phys. Rev. Lett. **26**, 1448 (1971).
[12] H.G. Bingham, M.L. Halbert, D.C. Hensley, E. Newman, K.W. Kemper, and L.A. Charlton, Phys. Rev. C **11**, 1913 (1975).
[13] D. Mikolas, Michigan State University Annual Report, 1987 (unpublished).
[14] W.D.M. Rae, A.J. Cole, B.G. Harvey, and R.G. Stokstad, Phys. Rev. C **30**, 158 (1984).
[15] K.W. Kemper and J.D. Fox, Nucl. Instrum. Methods **105**, 333 (1972).
[16] F. Ajzenberg-Selove, Nucl. Phys. **A413**, 1 (1984).
[17] D.D. Caussyn, Ph.D. thesis, Florida State University, 1990.
[18] A.M. Lane and R.G. Thomas, Rev. Mod. Phys. **30**, 257 (1958).
[19] A.R. Barnett, D.H. Feng, J.W. Steed, and L.J.B. Goldfarb, Comput. Phys. Commun. **8**, 377 (1974).
[20] J.A. Nelder and R. Mead, Comput. J. **7**, 308 (1964).
[21] F.C. Barker, Can. J. Phys. **61**, 1371 (1983).
[22] J.J. Kroepfl and C.P. Browne, Nucl. Phys. **A108**, 289 (1967).
[23] G.D. Symons and P.B. Treacy, Phys. Lett. **2**, 175 (1962).
[24] J.B. Marion, T.W. Bonner, and C.F. Cook, Phys. Rev. **100**, 91 (1955).
[25] R.J. Slobodrian, H. Bichel, J.S.C. McKee, and W.F. Tivol, Phys. Rev. Lett. **19**, 595 (1967).
[26] F.C. Barker and P.B. Treacy, Nucl. Phys. **38**, 33 (1962).